Journal of Analytical and Applied Pyrolysis 170 (2023) 105908

Contents lists available at ScienceDirect

Journal of Analytical and Applied Pyrolysis

journal homepage: www.elsevier.com/locate/jaap

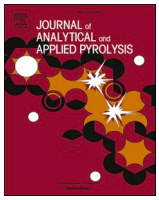

Experimental and kinetic study of high pressure pyrolysis of n-dodecane

Li Yikai [a], Jiahe Zhang [a,b], Li Yujun [b,c], Dawei Zhang [b], Naifu Cui [b], WU Kun [b], Taichang Zhang [b,c,*], Xuejun Fan [b,c]

[a] School of Mechanical Engineering, Beijing Institute of Technology, Beijing 100081, People's Republic of China
[b] State Key Laboratory of High Temperature Gas Dynamics, Institute of Mechanics, Chinese Academy of Sciences, Beijing 100190, People's Republic of China
[c] School of Engineering Science, University of Chinese Academy of Sciences, Beijing 100149, People's Republic of China

ARTICLE INFO

Keywords:
N-dodecane
High pressure pyrolysis
Reaction kinetics
Mechanism optimization
RMG

ABSTRACT

In this paper, a novel two-stage heating system of hydrocarbon fuel was used to simulate the fuel temperature, pressure and fuel residence time in cooling channels of an actively cooling scramjet, wherein the high-pressure pyrolysis of n-dodecane, a surrogate fuel, was experimentally studied. The fuel cracking experiment was carried out in the temperature range of 830–930 K and at a relatively constant pressure of 40 atm. When the pyrolysis temperature was below 890 K, the main pyrolysis products were macromolecular olefin. With the increase of pyrolysis temperature, the cracking degree of n-dodecane and the proportion of small olefin and alkane increased, and the cracking degree reached 53.5% at the pyrolysis temperature of 930 K. The proportion of each gas product is almost constant in the whole temperature range except the lowest temperature of 830 K, while the proportion of each liquid product to the total liquid products shows the same phenomenon. A preliminary detailed chemical kinetics model of 145 substances and 2024 reactions was established with RMG. The reaction mechanism generated by RMG and several published n-dodecane cracking reaction mechanisms were used in CHEMKIN simulation, respectively. By comparing the results of the experiment and the kinetic model, the obvious differences were observed and reasons were analyzed. On this basis, the RMG kinetic model was further optimized, and achieved in good accordance with the experimental results. The decomposition pathways of n-dodecane were further illustrated through the analysis of reaction flux. The primary decomposition of n-dodecane is mainly through the H-abstraction reaction with small-molecule free radicals, especially CH_3 and C_2H_5. The H-abstraction reaction results into six isomers of n-dodecyl. The consumption of n-dodecyl is mainly through H-shift isomerization and β-scissions, which mainly influence the distributions of pyrolysis products.

1. Introduction

The active cooling ramjet uses cooling channels in the wall of the engine chamber through which fuel flows before it is injected into the combustion chamber, taking away some of the heat from the wall and keeping the wall temperature within the permissible range. This is an important and effective method for hypersonic vehicle engine thermal management. In this process, the temperature and pressure of the hydrocarbon fuel are gradually rising due to absorption of heat from the wall. In fact, the extreme heat load of a supersonic combustor will cause the temperature of the hydrocarbon fuel to exceed 800 K, and the fuel pressure is usually controlled in the range of 30–60 atm. Under the conditions of high temperature and high pressure, the fuel will be pyrolyzed and in a cracking state [1].

The cracking of hydrocarbon fuel not only determines the cooling effect and pyrolytic carbon deposition in the cooling channel but also affects the flame stability and heat release distribution in the combustion chamber after the cracked fuel is injected into the combustor [2]. The study of the high-pressure pyrolysis and chemical kinetics of hydrocarbon fuels can reveal the mechanism of high-pressure pyrolysis of hydrocarbon fuels, furthermore quantify the fuel heat transfer in the engine cooling passage and the fuel composition entering the combustion chamber, facilitating the design of active cooling engine combustor [3,4]. However, the components of aviation kerosene are so complex that it is difficult to study directly the chemical kinetics of aviation kerosene. Under the condition that the chemical and physical properties are similar to those of the actual fuel, experimental studies using surrogate fuels are simple and efficient [5]. At present, 3–5 surrogate fuels,

* Corresponding author at: State Key Laboratory of High Temperature Gas Dynamics, Institute of Mechanics, Chinese Academy of Sciences, Beijing 100190, People's Republic of China.
E-mail address: taichang@imech.ac.cn (T. Zhang).

https://doi.org/10.1016/j.jaap.2023.105908
Received 9 November 2022; Received in revised form 17 January 2023; Accepted 4 February 2023
Available online 7 February 2023

which represent alkanes, cycloalkanes and aromatic hydrocarbons, are generally studied instead of kerosene. As the main component of aviation kerosene, n-dodecane is an important surrogate fuel of n-alkanes [6–8].

The pyrolysis of n-dodecane has been extensively studied. The experimental parameters are listed in Table 1. Yoon et al. studied the pyrolysis of n-dodecane in a batch reactor at a pressure of 10 atm and a temperature range of 523–673 K [9,10]. On this basis, Dahm et al. conducted pyrolysis experiments of n-dodecane at higher temperatures of 950, 1000 and 1050 K, and established a detailed kinetic model containing 1173 reactions [11]. Herbinet et al. conducted experiments with n-dodecane at a temperature range of 773–1073 K, residence times of 1–5 s, atmospheric pressure, and optimized the chemical mechanism [3]. Westbrook et al. established a detailed reaction mechanism suitable for the pyrolysis and combustion of paraffins from n-octane to n-hexadecane. The mechanism has been verified by some experimental and calculation data, which has greatly promoted the development of the pyrolysis mechanism of macromolecular hydrocarbon fuels [12]. Then Banerjee et al. established the pyrolysis and combustion mechanism of n-dodecane at a higher temperature range of 1000–1300 K and atmospheric pressure, and conducted more research on combustion on the basis of pyrolysis [13]. In terms of global mechanism research, Zhang et al. conducted a comprehensive study on the pyrolysis of n-dodecane under supercritical pressure and conducted kinetic modeling within the cracking zone. A global mechanism can describe the kinetic relationship of cracking phenomena observed experimentally, which is a practical solution in the simulation [14].

In summary, studies on the pyrolysis of n-dodecane were mainly performed in pressure range of 1–10 atm, while the high-pressure pyrolysis experiments are lacking. The application of the current detailed kinetic model to high pressure conditions needs to be verified, so it is necessary to carry out the pyrolysis research of n-dodecane under high pressure conditions. High-pressure pyrolysis reaction mechanism for some hydrocarbon fuels were developed, and whether the relevant model can be extended to the high-pressure pyrolysis of n-dodecane also needs to be studied. Jiang et al. established a differential overall reaction model with varying stoichiometric coefficients for the thermal cracking of n-decane under supercritical pressure [15]. Wang et al. studied the pressure effect of pyrolysis of n-decane under supercritical pressure and established a related pressure model [16]. Zhang et al. established a molecular reaction model for the thermal cracking of n-decane under supercritical pressure, and demonstrated the important role of the kinetic model in the simulation of the heat transfer process of supercritical cracking [17].

The work in this paper includes the setup of a heating device capable of more accurately simulating the active cooling of the fuel in the scramjet engine such as fuel temperature, residence time and cracking degree. A detailed kinetic model was established with RMG. The reaction mechanism generated by RMG and several published reaction mechanisms of n-dodecane pyrolysis in the literature were compared, and the results were validated against the experimental data. The reason for the difference is analyzed, and the mechanism of RMG is further optimized, which points out the direction of improving the simulation model and the chemical kinetics mechanism.

Table 1
Studies on the pyrolysis of n-dodecane relevant hydrocarbon fuels.

Researchers	Fuel	Temperature/K	Pressure/atm	Residence time
E.M.Yoon et al.[9,10]	Jet fuels and similar hydrocarbon mixtures	523–673	10	3 h、6 h
K.D.Dahm et al.[11]	n-Dodecane	950、1000、1050	1	0–0.2 s
Olivier Herbinet et al.[3]	n-Dodecane	773–1073	1	1–5 s
Westbrook et al.[12]	n-Alkane:C_8-C_{16}	800–1100	1	1–5 s
Sayak Banerjee et al.[13]	n-Dodecane	1000–1300	1	~ 40 ms
Zhang et al. [14]	n-Dodecane	723–1003	30	-

2. Research methodology

2.1. Fuel heating and delivery system

The high-pressure pyrolysis experiment of n-dodecane in this work was conducted on a novel two-stage heating system for hydrocarbon fuel in Institute of Mechanics, Chinese Academy of Sciences.

The schematic of two-stage fuel heating system is shown in Fig. 1. Before the experiment, n-dodecane is pumped into the storage-type first-stage heater, which preheats the fuel directly using heating rods and controls the hydrocarbon fuel at 563–573 K. To avoid fuel coking in the heat stage, the flow residence time in the second heating stage is elaborately controlled during which the fuel can be heated to temperature of 773–1003 K. The specific heating temperature is set according to the required experimental conditions. During the experiment, n-dodecane is pressurized in the first-stage heating system with nitrogen, and the pressure is controlled by a pressure regulator. Then, open the valve and delivery the n-dodecane to the second-stage heater. The final cracked product is firstly measured and controlled by the flowmeter [2], and then enters the condenser. After condensing, the gaseous and liquid cracking products are collected separately, and then stored separately through dedicated gas storage bags and sampling bottles. Finally, the components of pyrolytic gas and liquid collections were analyzed by the gas chromatography-mass spectrometry (GC-MS). The mixed samples were separated into individual components under suitable chromatographic conditions and then identified by mass spectrometry, finally, the data is processed. The instrument is GC-MS QP2010 Ultra (Shimadzu, Kyoto, Japan), which uses double-filament structure, ion source temperature 493 K, carrier gas is high-purity helium, flow rate is 1 ml/min. The uncertainty is estimated to be ± 10% for all species.

Because the fuel cracking degree is proportional to the fuel residence time at high temperatures, the fuel heating history should be alleviated. To accurately simulate the fuel heating history in the active cooling channels, a novel second stage heater is developed. The second stage heating section is heat sink heating, and the diameter and length are basically as same as the cooling channel in the scramjet engine wall. The total power of the entire second stage heater is 4 kW, and there are 18 fuel passages with the diameter of 2 mm and the length of 1000 mm. The metal shell of the heater is made of steel, and the heat sink block is made of 310 S high-temperature stainless steel. The maximum heating temperature of the superalloy heat sink block is 1123 K. The flow rate range in the heater is 30–80 g/s. The heating temperature of the fuel can be controlled within the range of 800–1000 K, and the corresponding pressure is within the range of 3–6 MPa.

Fig. 2(a) shows a schematic longitudinal cross-sectional view of the second-stage heater. The second-stage heater includes fuel inlet 1, fuel distribution manifold 2, heating rod 4, fuel passage 5, and metal shell 3. Metal shell 3 is formed by a high-temperature alloy heat sink block 7 arranged in the inner cavity, and heating rod 4 is installed through the inside of the high temperature alloy heat sink block 7. The inside of the metal shell 3 contains a fuel distribution manifold 2 and a fuel channel 5, and the end of the fuel channel 5 is provided with a fuel outlet 11. The fuel enters the distribution manifold along the fuel inlet 1, flows into the fuel channel 5 through the distribution cavity, and then flows out along fuel outlet 11. Before the experiment, the second-stage heater preheats high temperature alloy heat sink block 7 using heating rod 4 which passes through cylindrical high-temperature alloy heat sink block 7. The

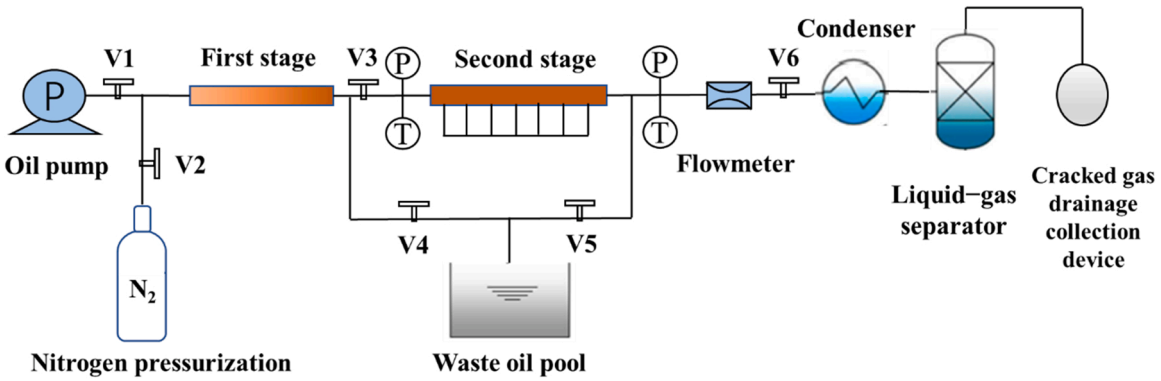

Fig. 1. Schematic of two-stage fuel heating system.

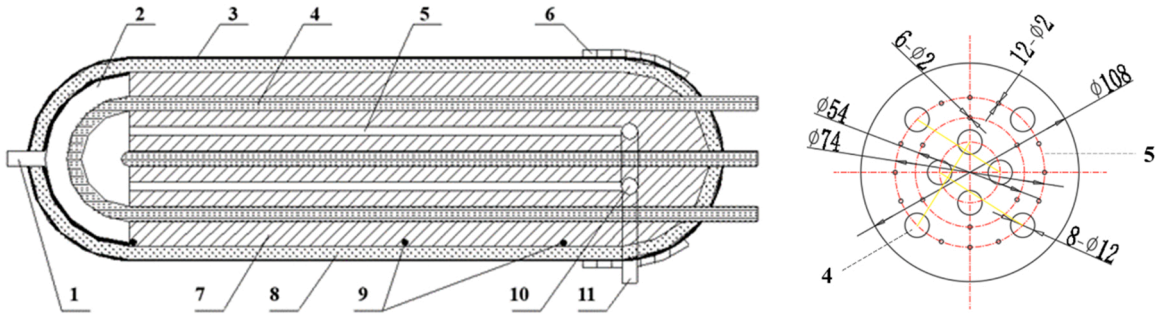

Fig. 2. (a) schematic diagram of the longitudinal cross section of the second-stage heater. (b) schematic diagram of the radially cross section of the second-stage heater. (1) fuel inlet; (2) fuel distribution manifold; (3) metal shell; (4) heating rod; (5) fuel channel; (6) heating belt; (7) high temperature alloy heat sink block; (8) thermal insulation material; (9) thermocouple; (10) confluence tank; (11) fuel outlet.

heating pipe of two-stage heating system adopts straight pipe. Although the conversion of fuel pyrolysis is lower than S-bend tube [18], it is closer to the true cooling channel shape and can produce less carbon deposits.

The outer sidewall of the metal shell close to the outlet end is wound with a heating belt, and several thermocouples are arranged on the front, middle and outer walls of the outlet end of the high-temperature alloy heat sink block, respectively. It should be noted that, in view of the uneven heater center temperature and outlet temperature in the previous design, this design has improved the design of the secondary heater. Specifically, the hollow oil collecting cavity of the original oil outlet is filled with a stainless-steel heat sink, and the newly filled heat sink block is heated. After the oil exits each flow channel in the heating section, it is first filled in the stainless-steel heat sink for collection and flows out after confluence. In addition, independent heating is added on the outlet side to make the temperature of the middle part of the heat sink and the outlet part consistent.

Fig. 2(b) shows the schematic diagram of the radially cross section of the second-stage heater. Heater rods and fuel passages are also shown. The diameter of the heating rod insertion hole is larger than that of the elongated hole, and the heating rod is inserted in the heating rod insertion hole.

In order to be closer to the actual situation, the end of the heater is also enclosed by a heat sink manifold, and it is also electrically heated at its end. At the same time, aluminum silicate fiber thermal insulation material is added outside the heater shell, and the thermal conductivity of the thermal insulation material is 0.03 W/m•K. This ensures that the temperature at the outlet of the heater is basically the same as the core temperature, which can meet the experimental requirements.

The temperature of the fuel flowing through the passage is simulated by using a one-dimensional solid-gas-liquid coupling analysis programme developed for simulating the active cooling effect [19]. The diameter of the fuel channel in the second heater is 2 mm, the initial temperature of the fuel is 573 K, and other conditions are set according to Table 2. As exhibited in Fig. 3, it can be found that under the condition of higher wall temperature, the flow distance required for the fuel temperature to reach 800 K is shorter and the length of the reaction tube for subsequent cracking is longer. According to the experimental results, the cracking onset temperature of n-dodecane is about 800 K. In this process, the wall temperature of the heat sink is assumed to be constant as the fuel flows since the heat sink is sufficiently large.

During the experiment, the purity of the n-dodecane sample was 99.0% measured by Tsinghua University Analysis Center, and the pressure sensor used the CYB-10S pressure sensor produced by AVIC Electromechanical Technology Co., Ltd., with an accuracy of ± 0.1%. The temperature sensor uses a K-type thermocouple with an uncertainty of ± 5 K.

Figs. 4 and 5 show the temperature and pressure changes of the n-dodecane flowing through the pipeline at 930 K and 40 atm test conditions, respectively. During the experiment, the fuel valve was opened at 5.9 s and closed at 11.9 s for fuel injection. And the valve V3 before the secondary heater was opened at 8 s. As seen from the diagram, the temperature and pressure are basically stable during the test time, so the experiment is accurate and reliable.

2.2. Flow reactor modeling

The total length of the second heater section is 1050 mm. Calculated by the one-dimensional fluid-solid coupling heat transfer program, the n-dodecane can reach 800 K within 210–400 mm from the pipe entrance under different temperature conditions, which is approximately considered as the beginning of cracking. At 800 K and 40 atm, the density of n-dodecane, denoted as ρ_0, is 161 kg/m^3, which is calculated by REFPROP (Reference Fluid Thermodynamic and Transport Properties

Table 2
Experimental conditions of high pressure n-dodecane pyrolysis.

Fuel	Mean fuel temperature/K	Experiment sampling time/s	Fuel pressure/atm	Flow rate/ (g/s)
n-dodecane	833	6	39.7	72.0
	863	6	38.9	63.6
	882	6	39.7	59.1
	900	6	39.7	52.3
	917	6	39.7	45.3
	925	6	39.2	42.6
	930	6	39.2	40.3

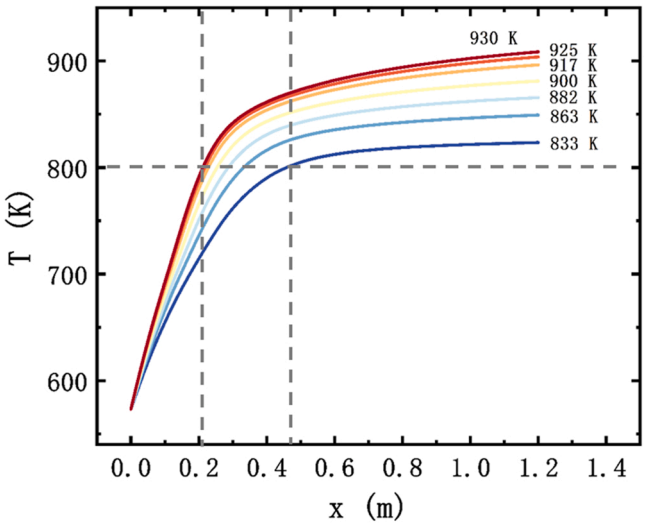

Fig. 3. Fuel temperature distribution in the channel along the flow direction.

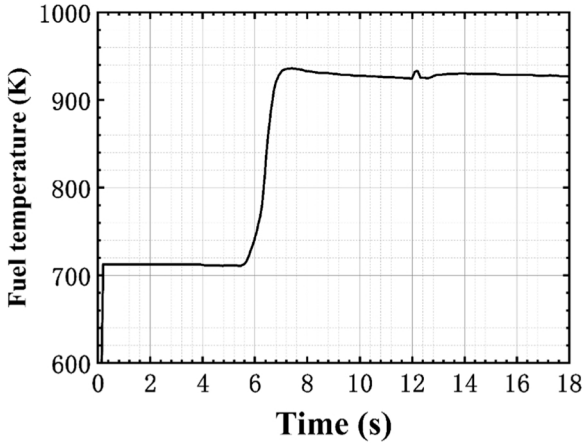

Fig. 4. Temperature variation of n-dodecane at 930 K and 40 atm experimental condition.

Database). Considering that there is a 200 mm pipeline between the secondary heater and the last shutoff valve, the total pipeline length is 1250 mm.

Through the experimental data, the average molar mass M_w of the reaction products (pyrolysis gas and liquid) can be calculated.

Numerous equations of state have been proposed to predict and correlate the properties of fluids. Among them, cubic equations of state (EOSs) have played a major role in the development of fluid state theories as well as modeling fluid behavior for practical purposes. Cubic EOSs are the most frequently used equations of state for practical applications, because they offer the best balance between accuracy, reliability, simplicity, and speed of computation [20]. The Peng-Robinson

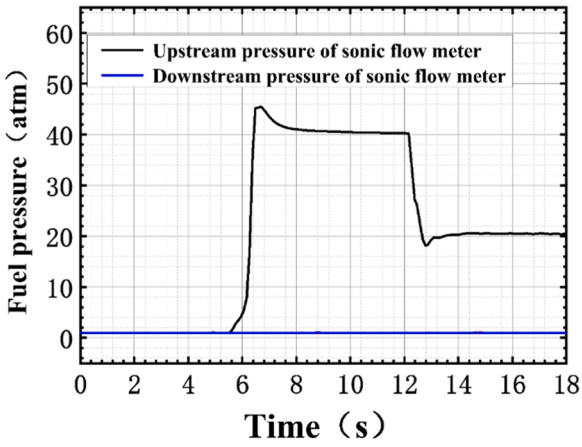

Fig. 5. Pressure change of the n-dodecane at 930 K and 40 atm experimental condition.

(PR) EOS, developed in 1976 [21], is probably the most frequently used cubic EOS in practical applications.

In order to obtain more accurate information such as the density of the cracked material in the supercritical state, we use the Peng-Robinson EOS to solve it.

$$P = \frac{RT}{v-b} - \frac{a(T)}{v(v+b)+b(v-b)} \tag{1}$$

where P is pressure, T is temperature, v is the specific volume, R is the gas constant, and $a(T)$ and b are the parameters of the EOS. At constant P and T, the equation will take the form of a cubic equation in v and can be solved for v using any standard analytical or numerical technique [22]. The limitations on critical point lead to the following relations for the PR EOS parameters [21].

$$b = 0.07780\frac{RT_c}{P_c} \tag{2}$$

$$a(T) = [0.45724\frac{R^2{T_c}^2}{{P_c}^2}]\alpha(T) \tag{3}$$

where subscript c indicates critical property and $\alpha(T)$ is temperature dependent, which should be chosen such that the vapor pressures predicted by the EOS at temperatures other than the critical one are accurate. The form proposed by Peng and Robinson is [21].

$$\alpha(T) = [1 + k(1 - {T_r}^{1/2})]^2 \tag{4}$$

where $T_r = T/T_c$ is the reduced temperature, $k = 0.37464 + 1.54226w - 0.26992w^2$, and w is the acentric factor. This form of $\alpha(T)$ was first proposed by Soave for the Redlich-Kwong (RK) EOS [23].

The average molar mass in the table is calculated by the mass fraction of each pyrolysis product measured in the GC-MS, and the flow rate is calculated by the weight of the pyrolysis liquid and the volume of the pyrolysis gas. Finally, the product density at the exit is calculated by

Peng-Robinson EOS Table 3.

Suppose the flow velocity of n-dodecane is v_1 when the fuel temperature just reaches 800 K, and v_1 can be obtained by using equation

$$q_m = \rho_0 v_1 A \quad (5)$$

The velocity of the reaction product at the outlet is v_2, which can be obtained by the similar equation. In this paper, it can be approximated that the average flow velocity $\bar{v}$ [24] is the linear average velocity of v_1 and v_2, and finally, the reaction time in the heating pipe can be obtained according to the total pipe reaction length. All flow data are shown in Table 4. Parameters in the following simulation can be set according to the above pressure, temperature and reaction time and other operating condition information.

2.3. Detailed kinetic models

In this paper, the pyrolysis mechanism and concentration distribution of n-dodecane pyrolysis product under high pressure are studied based on the open-source chemical reaction mechanism generator RMG (Reaction Mechanism Generator: Automatic construction of chemical kinetic mechanisms) developed by Connie W. Gao et al. [25]. It uses known chemical knowledge stored in databases and parameter estimation methods to generate detailed chemical kinetics mechanisms, which can further be used to simulate and predict the macro variables of interest in CHEMKIN. By searching for the reaction families that may occur in molecules, RMG puts species with higher critical fluxes and their related reaction into a core kinetic model based on the path flux algorithm [26]. By means of database comparison, the rate rule and group contribution method [27], the thermal properties of the species and the rate parameters of the reaction mechanism were predicted. At present, RMG supports only constant temperature and pressure reactor settings for gas phase systems. Although its reactor model is relatively simple (equivalent to the 0-d model), RMG has been used in study of JP-10 [28].

CHEMKIN is a software package whose purpose is to facilitate the formation, solution, and interpretation of problems involving elementary gas-phase chemical kinetics. It provides an especially flexible and powerful tool for incorporating complex chemical kinetics into simulations of fluid dynamics. The package consists of two major software components: an Interpreter and a Gas-Phase Subroutine Library. The Interpreter is a program that reads a symbolic description of an elementary, user-specified chemical reaction mechanism. One output from the Interpreter is a data file that forms a link to the Gas-Phase Subroutine Library. This library is a collection of about 100 highly modular Fortran subroutines that may be called to return information on equation of state, thermodynamic properties, and chemical production rates[29].

Using the advantages of CHEMKIN, we can carry out the simulation study of n-dodecane pyrolysis under high pressure. And four detailed kinetic models have been selected for comparing the experiment data with the Plug stirred reactor (PSR) model simulations.

According to the parameter settings shown in Table 5, the corresponding mechanisms can be obtained by running RMG. In addition to the kinetic models automatically generated by RMG, there are several other detailed and semi-detailed kinetic models involving heavy n-alkanes such as n-dodecane. Lawrence Livermore National Laboratory (LLNL) developed a detailed kinetic model for paraffins from n-octane to n-hexadecane based on the mechanism of n-heptane and isooctane, taking into account high temperature and low temperature reaction pathways [12]. The CRECK group at the Politecnico di Milano used the program MAMOX++ to automatically generate a semi-detailed kinetic model for the pyrolysis oxidation of several species including n-dodecane [30]. The Jet Surrogate Fuel (JetSurF) model includes the oxidation chemistry of n-alkanes to n-dodecane and a lumped low-temperature chemistry sub-model for the oxidation of n-alkanes in the negative temperature coefficient (NTC) region[31].

Table 3
Experimental parameters.

Mean Fuel temperature /K	Average molar mass /(kg/mol)	Pressure /atm	Flow rate/ kg/s	Reaction product density at outlet/ (kg/m^3)
833	0.160	40	0.072	82.1
863	0.147	40	0.636	73.7
882	0.130	40	0.591	64.7
900	0.107	40	0.523	53.1
917	0.081	40	0.453	40.2
925	0.071	40	0.426	35.2
930	0.063	40	0.403	31.2

Table 4
Flow data in the reaction pipeline.

Mean oil temperature/ K	Reaction tube length/m	v_1/ (m/ s)	v_2/ (m/ s)	Average speed $\bar{v}$/ (m/s)	Reaction time/s
833	0.790	7.96	15.5	11.7	0.067
862	0.916	7.03	15.3	11.2	0.082
882	0.962	6.54	16.2	11.3	0.085
900	0.997	5.78	17.4	11.6	0.086
917	1.022	5.01	19.9	12.5	0.082
925	1.033	4.71	21.4	13.1	0.079
930	1.040	4.46	22.8	13.6	0.076

3. Experimental results

3.1. Pyrolysis gas composition

The cracked gas contains various small molecules of olefins (ethylene, propylene, isomers of butene), alkanes (ethane, propane, isomers of butane and pentane) and hydrogen.

The mole fraction of each cracked gas is the ratio of moles of the cracked gas to the sum of moles of the cracked gas. As shown in Fig. 6, the mole fraction of ethylene is the highest, the mole fractions of methane, ethane, propane, and propylene are roughly equivalent, and the mole fractions of other substances are relatively small.

It should be noted that in the mass fraction diagram, the mass fraction of each pyrolysis gas is the proportion of the pyrolysis gas to the total pyrolysis products. Under different conditions of cracking gas, the mass fractions of ethylene and propylene are the highest, followed by ethane and propane, the mass fraction of olefins and alkanes with slightly larger molecules is smaller (The mass fraction of n-butene is the highest among the isomers of butene, and the mass fraction of n-butane is the highest among the isomers of butane), and the mass fraction of hydrogen is minimal Fig. 7.

Fig. 8 shows on the whole the proportion of each gas product change in a little range in the whole temperature range except the lowest temperature of 830 K. Actually, the proportion of ethylene at 833 K is obviously lower than that at other temperatures, while C4 species at 833 K is relatively higher than that at other temperatures. The difference of the proportion becomes smaller with the temperature increasing. The possible reason is that the main reaction paths change with the temperature increasing.

3.2. Pyrolysis liquid composition

The pyrolysis liquid contains macromolecular normal olefins (carbon number from 6 to 12), normal alkanes (carbon number from 7 to 13), benzene, and aromatic compounds. In the cracking solution under different working conditions, normal olefins account for the largest proportion, and the carbon number is mainly concentrated in 6–10. Secondly, n-alkanes occupy a certain proportion, the mass fractions of benzene and aromatic compounds are relatively small, and the mass

Table 5
Parameter settings of RMG and CHEMKIN.

Reactant	Reaction temperature/K	Pressure/atm	Reaction time/s	Tolerance in RMG
n-dodecane	800 830 860 890 920 950 970 1000	40	0.1	0.05

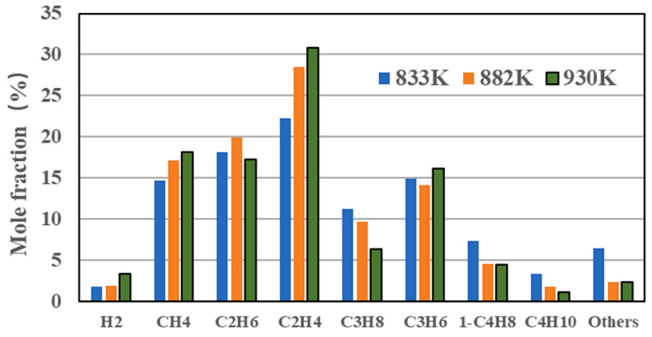

Fig. 6. Mole fraction of cracked gas under different experimental temperature conditions.

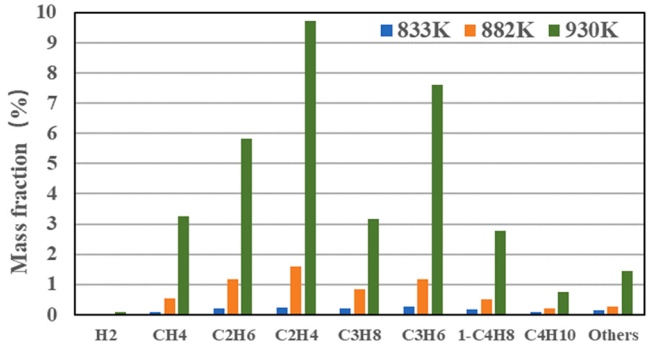

Fig. 7. Mass fraction of cracked gas under different experimental temperature conditions.

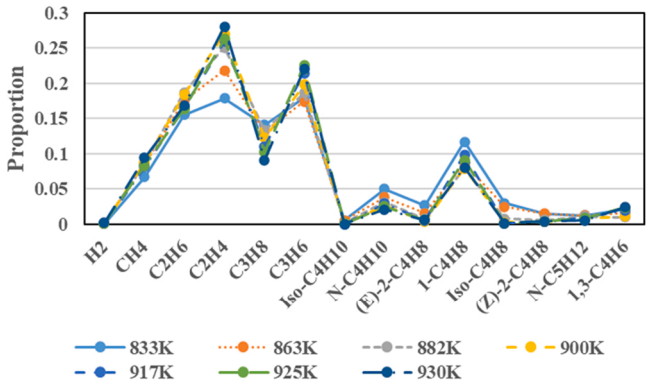

Fig. 8. The mass proportion of each gas product to the total gas products at different temperatures.

fractions of naphthalene and indene are the smallest.

Liquid products were analyzed by the gas chromatography-mass spectrometry (GC-MS). The mass fraction of each pyrolysis product in the pyrolysis liquid are shown in the table. The full two-dimensional gas chromatograms of n-dodecane pyrolysis products are presented as supplementary materials Table 6.

Fig. 9 shows the liquid phase product proportion changes in a small range with the increase of temperature except the operating condition of 833 K. This shows that the liquid product maintains a fixed proportion in the total product at different temperatures. For the case of 833 K, the cracking degree is too small to have a certain regularity.

4. Model comparisons

The differences between the experimental results under high-pressure and the low-pressure experiments were compared in two aspects. According to the results of previous experiments [11], the conversion of n-dodecane at atmospheric pressure is obviously lower than that at 40 bar at the same residence time and temperature. Moreover, at the similar cracking degree and residence time, the mole fractions of the products at atmospheric pressure and at 40 bar are different. For example, the mole fractions of methane and ethane at atmospheric pressure are much lower than those at 40 bar, while the mole fraction of ethylene is much higher than that at 40 bar. It demonstrates the differences of cracking paths between high and low pressures. Therefore, it is necessary to validate the current model and further develop the model for high-pressure condition.

This section compares the simulation results of the LLNL mechanism [12], the JetSurf mechanism [32], the CRECK mechanism [33] and the RMG mechanism with the experimental results, and finds the shortcomings of the RMG mechanism in simulation by analyzing the differences.

The experimental data show that the pyrolysis rate of n-dodecane is low when the temperature of n-dodecane is below 830 K and increases rapidly when the temperature is between 830 K and 930 K with the reaction time of 0.1 s. The highest conversion of n-dodecane was approximately 53.5% at an experimental temperature of 930 K. Through the comparison of experimental data and the simulation results of the four mechanisms, it can be found that the four mechanism curves and experimental data points have roughly the same trend, but the conversion rates of n-dodecane by the RMG, LLNL and JetSurf mechanisms are estimated to be smaller than the experimental result, and that of the CRECK mechanism is estimated to be larger. With increasing temperature, the deviation of the RMG mechanism simulation results from the experimental data becomes larger. It is worth noting that too high or too low estimations of the conversion rate of n-dodecane are related with the content of the corresponding products Fig. 10.

From the perspective of the types of gas phase products, the simulation results of the four mechanisms are not sufficient. They lack products such as butene isomers but include all major gas phase products, such as olefins (ethylene, propylene, 1-butene) and alkanes (methane, ethane, propane); from the perspective of gas phase product content, the simulation results of the four mechanisms are different with the experimental results in different degrees.

Regarding the results of olefins, in the temperature range of 830–930 K, the simulation curves of the four mechanisms have the same changing trends to the experimental results, and they all show a

Table 6
Mass fraction of each pyrolysis product in the pyrolysis liquid.

Name	n-dodecane sample	835 K	863 K	882 K	900 K	917 K	925 K	930 K
Benzene		0.03	0.03	0.04	0.08	0.1	0.19	0.2
Toluene				0.09	0.14	0.16	0.16	0.2
C2-benzene							0.11	0.13
C3-benzene							0.04	0.08
Indan							0	0.01
Indene							0.01	0.02
Naphthalene						0.03	0.04	0.06
Indene							0.09	0.09
Biphenyl							0.01	0.02
1-Heptene		0.52	0.88	1.56	2.81	4.05	5.35	4.72
1-Octene		0.31	0.88	1.58	2.66	3.80	4.77	4.50
1-Nonene		0.28	0.86	1.46	2.51	3.55	4.52	4.44
1-Decene		0.31	0.82	1.45	2.25	3.31	4.08	4.19
1-Undecene		0.19	0.33	0.62	1.00	1.49	1.84	1.99
1-Dodecene			0.10	0.23	0.26	0.42	0.49	0.57
Heptane			0.13	0.18	0.25	0.32	0.34	0.34
Octane		0.11	0.16	0.33	0.39	0.46	0.61	0.58
Nonane		0.11	0.17	0.36	0.41	0.49	0.58	0.56
Decane			0.05	0.16	0.12	0.15	0.18	0.20
Undecane	0.61	0.49	0.49	0.44	0.43	0.41	0.47	0.47
Dodecane	99.00	96.98	94.27	90.29	86.24	79.90	71.94	71.20
Tridecane	0.32	0.36	0.35	0.34	0.32	0.29	0.23	0.22
Tetradecane	0.07						0.02	0.03

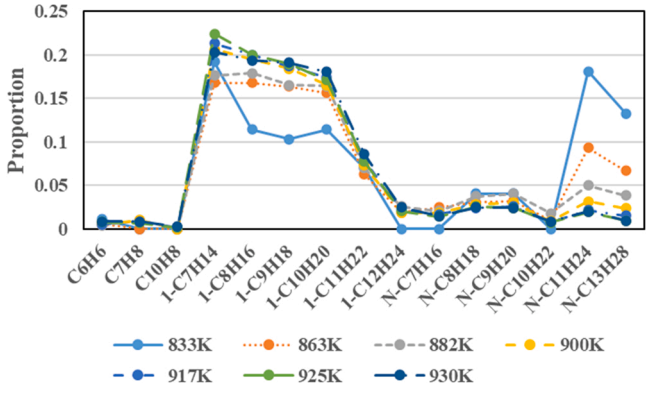

Fig. 9. The mass proportion of each liquid product to the total liquid products at different temperatures.

continuous upwards trend. However, the CRECK mechanism estimates the overall content of olefins on the high side, while the RMG, LLNL and JetSurf mechanisms under-predict the overall content of olefins. Among them, in the temperature range higher than 930 K, the LLNL mechanism shows a gentle upwards and downwards trend, which is different from the other three mechanisms. Overall, the calculated value of the CRECK mechanism is more consistent with the experimental results of ethylene and propylene, and the calculation of the RMG mechanism is more consistent with the experimental results of 1-butene. From the results of alkanes, the simulation curves of the four mechanisms show the same trend as the experimental results in the temperature range of 830–930 K. The JetSurf mechanism seriously underestimates the contents of ethane and propane, the LLNL mechanism seriously underestimates the contents of propane, the CRECK mechanism overestimates the total contents of alkanes, and the RMG mechanism underestimates the total contents of alkanes. When the temperature is higher than 930 K, the simulation result of propane by the CRECK mechanism will decrease, and the simulation curve of alkane by the other three mechanisms will increase continuously. In general, the calculated values of the CRECK mechanism are in good agreement with the experimental results of alkanes.

Overall, the calculated values of the CRECK mechanism and the RMG mechanism are in good agreement with the experimental values of the gas phase products, and the CRECK mechanism is more accurate. This shows that the CRECK mechanism and the RMG mechanism are relatively good in dealing with the related reactions of gas phase products during pyrolysis.

Many kinds of liquid products are produced in the experiment. In addition to containing the main liquid phase products 1-olefins, there are also some substances ignored in the simulation due to their small content, such as aromatic hydrocarbons (benzene, toluene, naphthalene) and some n-alkanes. The main liquid phase products 1-olefin (1-heptene, 1-octene, 1-nonene, 1-decene) and aromatic hydrocarbons are analyzed and compared. In the experimental data, the olefin content peaked at 925 K and then began to decline. According to the results of the 1-olefin comparison, the calculated values of the four mechanisms agree poorly with the experimental values. 1-heptene and 1-decene are overestimated by CRECK mechanism, while four kinds of 1-olefins are underestimated by the other mechanisms. According to the comparison results of mechanism and experiment, the relevant important reactions and relevant important products involved in the mechanism will be further studied Tables 7 and 8.

For aromatic hydrocarbons, benzene, toluene, and naphthalene appeared in the experiment, the content of aromatic hydrocarbon in the calculation of CRECK mechanism increased sharply with the increase of temperature, while the RMG mechanism only showed a small amount of benzene at 1000 K. There are no aromatic hydrocarbons in the LLNL mechanism or the JetSurf mechanism. Gascoin et al. found evidence of coke formation during the pyrolysis of n-dodecane [34]. Aromatic hydrocarbons are important raw materials in the coke production process [35], so the work below will continues to optimize the RMG mechanism for aromatic hydrocarbons predictions.

5. Mechanism optimization

Through the content of Section 4, it is found that the existing mechanisms such as LLNL, JetSurf and CRECK cannot well predict the decomposition process of n-dodecane under high pressure as there is a certain gap between the simulation results of the self-generated RMG mechanism and the experimental results. Therefore, this part will optimize the mechanism of the self-generated RMG mechanism to improve the high-pressure pyrolysis kinetic model of n-dodecane, and discuss the associated high-pressure pyrolysis process.

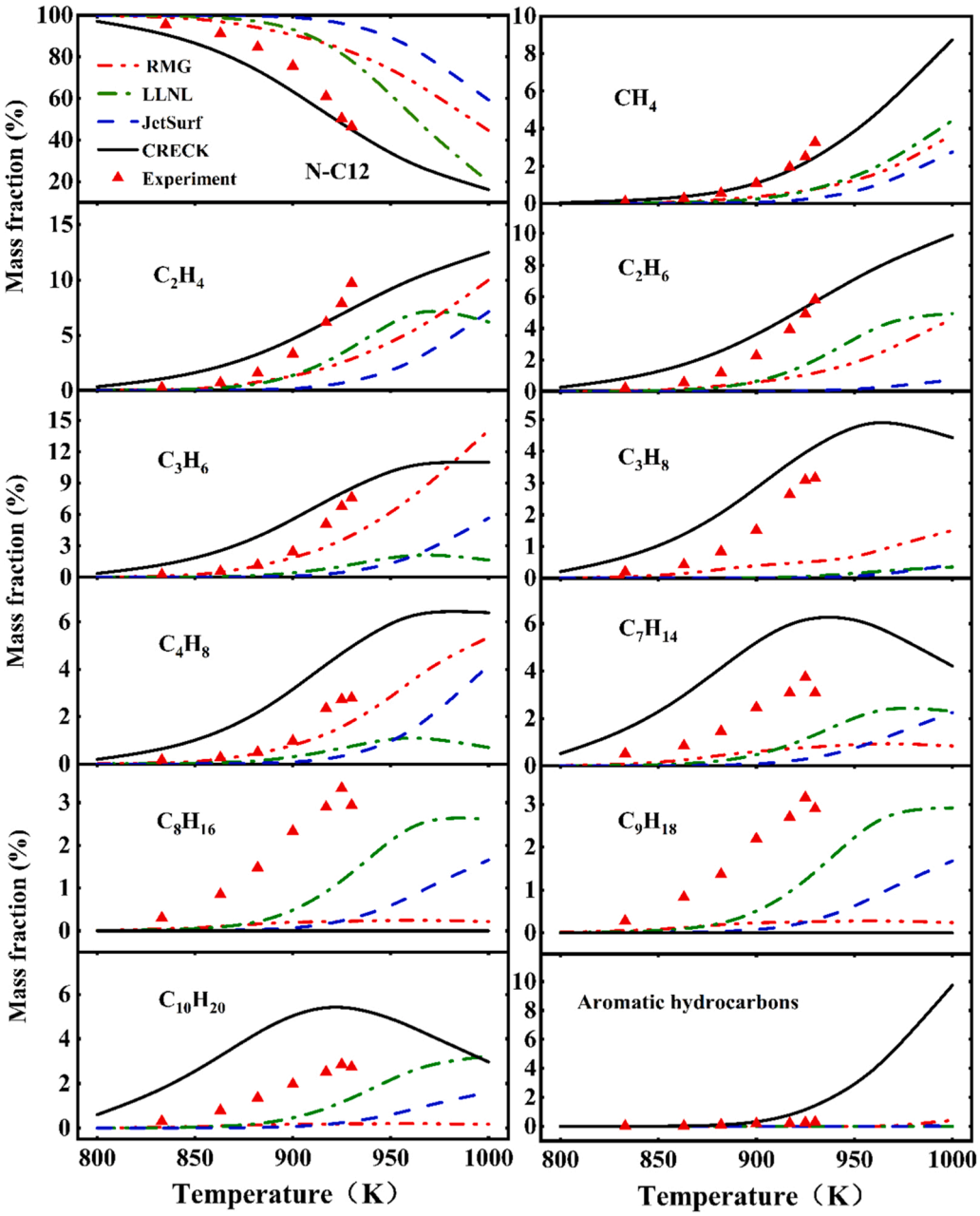

Fig. 10. Mass fraction of each pyrolysis product at different pyrolysis temperatures.

Table 7
The mass fraction of aromatic compounds under different temperature experimental conditions.

Name	Molecular formula	830 K	863 K	882 K	900 K	917 K	925 K	930 K
Benzene	C_6H_6	0.0294	0.0286	0.0364	0.0658	0.0669	0.1112	0.1027
Toluene	C_7H_8			0.0819	0.1152	0.1071	0.0936	0.1027
Naphthalene	$C_{10}H_8$					0.0201	0.0234	0.0308

5.1. Model modification

The process of parameter optimization depends on the uncertainty of quantization, because the rate coefficient can only be modified in the range of uncertainty in the process of parameter optimization. To this end, important reactions are usually first identified by sensitivity analysis under specific conditions. The rate parameters for these reactions were then iteratively modified within uncertainty to achieve good agreement between model and experiment. It is known that the most common way to adjust the reaction rate is to change the pre-exponential factor in the Arrhenius equation as a calibration target [36,37]. Based on the sensitivity analysis, some important reactions were identified, then the kinetic model of n-dodecane pyrolysis was improved by adjusting the pre-exponential factor.

The self-generated RMG mechanism contains 145 species and 2024 reactions, and is adjusted for reactions with a carbon number greater than 4 using an optimization program, with the adjustment range of pre-exponential factors of 0.25–4 for various reactions as suggested by Cai

Table 8
Adjusted reactions with the highest iteration frequency.

Type of reaction	Reaction	Pre-exponential factor adjustment multiplier
unimolecular decomposition reactions	1. n-$C_{12}H_{26}$ = C_2H_5 + 1-$C_{10}H_{21}$	4.00
	2. n-$C_{12}H_{26}$ = 1-C_3H_7 + 1-C_9H_{19}	4.00
	3. n-$C_{12}H_{26}$ = 1-C_5H_{11} + 1-C_7H_{15}	4.00
	4. n-$C_{12}H_{26}$ = 1-C_4H_9 + 1-C_8H_{17}	4.00
	5. n-$C_{12}H_{26}$ = 1-C_6H_{13} + 1-C_6H_{13}	4.00
H-abstraction reactions	6. CH_3 + n-$C_{12}H_{26}$ = CH_4 + 1-$C_{12}H_{25}$	4.00
	7. CH_3 + n-$C_{12}H_{26}$ = CH_4 + 2-$C_{12}H_{25}$	4.00
	8. CH_3 + n-$C_{12}H_{26}$ = CH_4 + 4-$C_{12}H_{25}$	4.00
	9. C_2H_5 + n-$C_{12}H_{26}$ = C_2H_6 + 3-$C_{12}H_{25}$	4.00
	10. C_2H_5 + n-$C_{12}H_{26}$ = C_2H_6 + 4-$C_{12}H_{25}$	4.00
	11. C_2H_5 + n-$C_{12}H_{26}$ = C_2H_6 + 5-$C_{12}H_{25}$	4.00
	12. C_2H_5 + n-$C_{12}H_{26}$ = C_2H_6 + 6-$C_{12}H_{25}$	4.00
	13. C_2H_5 + n-$C_{12}H_{26}$ = C_2H_6 + 2-$C_{12}H_{25}$	4.00
	14. C_2H_5 + n-$C_{12}H_{26}$ = C_2H_6 + 1-$C_{12}H_{25}$	4.00
	15. 1-C_3H_7 + n-$C_{12}H_{26}$ = C_3H_8 + 4-$C_{12}H_{25}$	4.00
	16. 1-C_3H_7 + n-$C_{12}H_{26}$ = C_3H_8 + 1-$C_{12}H_{25}$	4.00
	17. C_3H_5-a + n-$C_{12}H_{26}$ = C_3H_6 + 2-$C_{12}H_{25}$	4.00
	18. C_3H_5-a + n-$C_{12}H_{26}$ = C_3H_6 + 6-$C_{12}H_{25}$	4.00
	19. C_3H_5-a + n-$C_{12}H_{26}$ = C_3H_6 + 5-$C_{12}H_{25}$	4.00
reactions of alkyl radicals	20. 5-$C_{12}H_{25}$ = 1-C_6H_{12} + 1-C_6H_{13}	1.02
	21. 5-$C_{12}H_{25}$ = 1-C_3H_7 + 1-C_9H_{18}	2.53
	22. 4-$C_{12}H_{25}$ = C_2H_5 + 1-$C_{10}H_{20}$	3.25
	23. 6-$C_{12}H_{25}$ = 1-C_4H_9 + 1-C_8H_{16}	4.00
	24. 4-C_8H_{17} = C_2H_5 + 1-C_6H_{12}	4.00
	25. 1-C_5H_{11} = C_2H_4 + 1-C_3H_7	4.00
reactions of alkene and alkene radicals	26. 1-C_9H_{18} = C_3H_6 + 1-C_6H_{12}	0.25
	27. 1-$C_{10}H_{20}$ = C_3H_6 + 1-C_7H_{14}	0.25
	28. 1-C_8H_{16} = C_3H_6 + 1-C_5H_{10}	0.35
	29. C_2H_5 + C_3H_5-a = 1-C_5H_{10}	0.25
	30. 1-C_8H_{16} = C_3H_5-a + 1-C_5H_{11}	4.00

et al. [37].

Based on the sensitivity analysis of n-dodecane and its pyrolytic products in CHEMKIN at different temperatures, pre-exponential factors of 118 important reactions were modified during the optimization process. After optimization, the reactions were ranked according to the priority of the selected reactions in the iteration, and the first 25% of the reactions were selected as the results of the main presentation. Finally, the major 30 reactions in the optimization process were divided into the following four types: unimolecular decomposition reactions, H-abstraction reactions, reactions of alkyl radicals, and reactions of alkene and alkene radicals [38]. The following are the specific reaction and the adjustment of the pre-exponential factor.

For the unimolecular decomposition reactions, the pre-exponential factor is increased by 4 times, which enhances the decomposition rate of n-dodecane and the conversion rate of n-dodecane to a certain extent; for the H-abstraction reactions, the pre-exponential factors are increased to varying degrees, which will increase the reaction rate of the free radical and n-dodecane, thereby accelerating the pyrolysis process of n-dodecane; for the alkyl radical reaction type, the pre-exponential factors are increased to different degrees, which will promote the decomposition of macromolecular substances and accelerate the formation of small molecular substances; for the reaction types of olefin and olefin group, by adjusting the pre-exponential factor, the consumption rate of macromolecular alkenes in the product is reduced, which is beneficial to achieve agreement with the experimental results. We also note that it is not reasonable to adjust the pre-exponential factor of a single reaction only by considering sensitivity analysis. From the point view of kinetics, the pre-exponential factor according to the reaction category should be adjusted, and in this way, the kinetic consistency can be ensured.

The cracking degree of n-dodecane in high pressure pyrolysis is higher than that predicted by the original RMG mechanism and other mechanisms, although these published mechanisms have been validated in relatively low pressures. Similar phenomenon is also found in the high pressure pyrolysis of n-decane [38]. Some studies have shown that the reaction rate of free radicals with reactants is increased under high pressure [39], which should be one possible reason. Therefore, considering the importance of the H-abstraction reactions in the cracking process of n-dodecane, the pre-exponential factor of the H-abstraction reactions is uniformly raised by 4 times. The relevant reactions are shown in Table 9 below.

Table 9
Adjustments to H-abstraction reactions of n-dodecane.

Type of reaction	Reaction	Pre-exponential factor adjustment multiple
H-abstraction reactions	CH_3 + n-$C_{12}H_{26}$ = CH_4 + 2-$C_{12}H_{25}$	4.00
	CH_3 + n-$C_{12}H_{26}$ = CH_4 + 6-$C_{12}H_{25}$	4.00
	CH_3 + n-$C_{12}H_{26}$ = CH_4 + 3-$C_{12}H_{25}$	4.00
	CH_3 + n-$C_{12}H_{26}$ = CH_4 + 5-$C_{12}H_{25}$	4.00
	CH_3 + n-$C_{12}H_{26}$ = CH_4 + 1-$C_{12}H_{25}$	4.00
	CH_3 + n-$C_{12}H_{26}$ = CH_4 + 4-$C_{12}H_{25}$	4.00
	C_2H_5 + n-$C_{12}H_{26}$ = C_2H_6 + 3-$C_{12}H_{25}$	4.00
	C_2H_5 + n-$C_{12}H_{26}$ = C_2H_6 + 4-$C_{12}H_{25}$	4.00
	C_2H_5 + n-$C_{12}H_{26}$ = C_2H_6 + 5-$C_{12}H_{25}$	4.00
	C_2H_5 + n-$C_{12}H_{26}$ = C_2H_6 + 6-$C_{12}H_{25}$	4.00
	C_2H_5 + n-$C_{12}H_{26}$ = C_2H_6 + 2-$C_{12}H_{25}$	4.00
	C_2H_5 + n-$C_{12}H_{26}$ = C_2H_6 + 1-$C_{12}H_{25}$	4.00
	1-C_3H_7 + n-$C_{12}H_{26}$ = C_3H_8 + 3-$C_{12}H_{25}$	4.00
	1-C_3H_7 + n-$C_{12}H_{26}$ = C_3H_8 + 4-$C_{12}H_{25}$	4.00
	1-C_3H_7 + n-$C_{12}H_{26}$ = C_3H_8 + 5-$C_{12}H_{25}$	4.00
	1-C_3H_7 + n-$C_{12}H_{26}$ = C_3H_8 + 6-$C_{12}H_{25}$	4.00
	1-C_3H_7 + n-$C_{12}H_{26}$ = C_3H_8 + 2-$C_{12}H_{25}$	4.00
	1-C_3H_7 + n-$C_{12}H_{26}$ = C_3H_8 + 1-$C_{12}H_{25}$	4.00

According to the free radical reaction mechanism, the H-abstraction reactions occupies a very large proportion in the preliminary pyrolysis of n-dodecane, which will be mentioned in detail later. Expanding the pre-exponential factor of the H-abstraction reactions uniformly is beneficial to promote the pyrolysis process of n-dodecane and better simulate the experimental results.

Then, starting from the accuracy of fitting the reaction parameters of the RMG mechanism, some important reactions were selected in each reaction type to study the variation of the reaction rate constant with temperature.

It can be found from Figs. 11–14 that the rate constant of the original RMG mechanism is basically the same as the existing LLNL mechanism. In addition, the adjustment of the pre-exponential factor within the confidence interval resulted in a linear change of the rate parameter in the optimized mechanistic reaction within a reasonable range.

5.2. Comparison of optimized model with experimental results

Seven experimental operating conditions such as 833, 863, 882, 900, 917, 925, and 930 K were simulated in the PSR model of CHEMKIN, and the mass fractions of 12 main substances after the pyrolysis of n-dodecane were calculated. The experimental data, the original mechanism simulation data, and the optimized mechanism simulation data are compared. At the same time, considering the uncertainty of estimated residence time and the difference of the experimental reaction time under various temperature conditions calculated in Section 2.1, the residence time of 0.07 and 0.1 s was used in the optimized mechanism simulation respectively to present the influence of residence time uncertainty on the simulation results.

In Fig. 15, as compared to the original mechanism, the optimized mechanism has greatly improved agreement with the experimental results in the conversion of n-dodecane and the mass fraction of pyrolysis products. And from a kinetic point of view, modifications to the reaction classes ensured the consistency of the kinetics. It should be noted that there is still a large deviation between the results of aromatic hydrocarbons and the experimental values after optimization, which may be attributed to the lack of related mechanisms of aromatic hydrocarbons and certainly merits a further improvement in the future.

In terms of uncertainty, the results show that the cracking degree of n-dodecane and the mass fraction of some gas phase products are lower at low residence time than at large residence time, the mass fraction of the product at large residence time is lower than that at small residence time due to the further decomposition of the liquid product as the residence time increased.

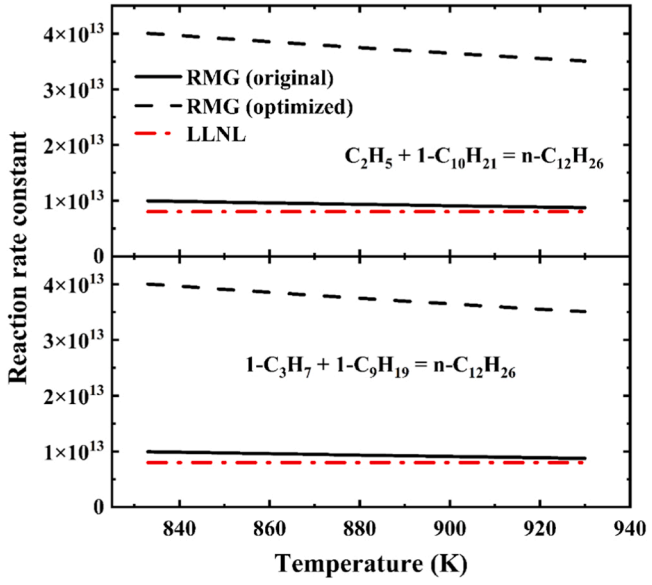

Fig. 11. Variation of the rate constant of unimolecular decomposition reaction with temperature.

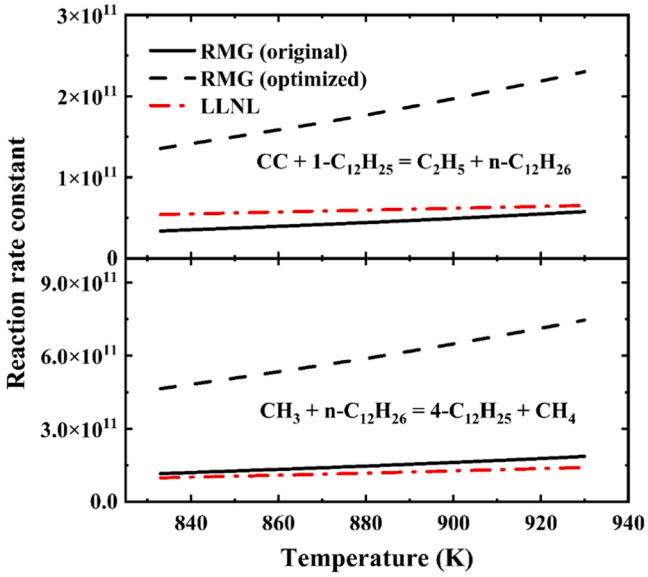

Fig. 12. Variation of H-abstraction reactions rate constant with temperature.

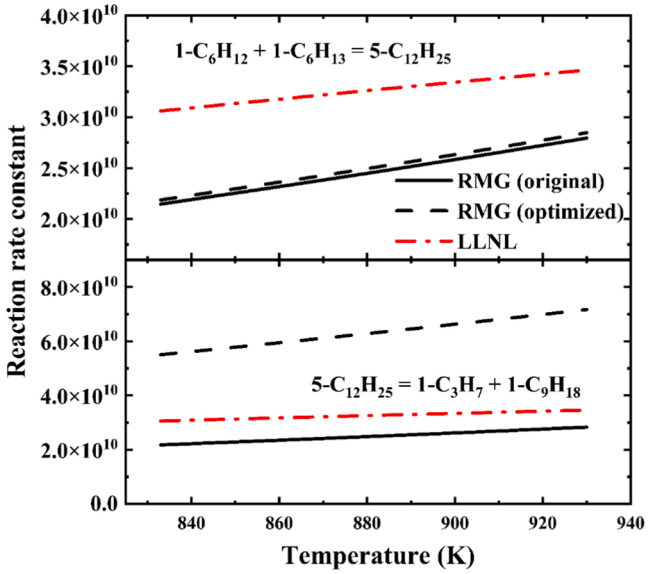

Fig. 13. The reaction rate constant of alkyl radicals as a function of temperature.

5.3. Preliminary decomposition of n-dodecane under high pressure

The primary decomposition of n-dodecane is mainly through the H-abstraction reaction with small-molecule free radicals. The reaction flux is shown in Fig. 16. Based on the rate of production (ROP) analysis, n-dodecane passes through 6 carbon atoms at different positions. The H-abstraction reaction is initially decomposed into 6 isomers of n-dodecyl. According to the free radical reactions, under high pressure, the collision of free radicals with high concentrations of reactants is enhanced, and the bimolecular reaction is superior to the free radical decomposition reaction [39]. Among them, the reaction rate constant of generating $1\text{-}C_{12}H_{25}$ is larger than that of other reactions, so the generation ratio is higher, while the other n-dodecyl isomers are similar.

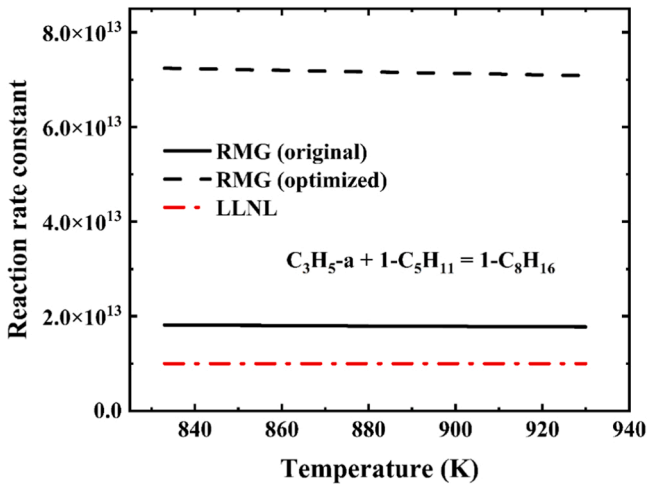

Fig. 14. The reaction rate constant of alkene and alkene group as a function of temperature.

As shown in Fig. 17, based on the production rate (ROP) analysis, n-dodecane collides with four free radicals in the initial decomposition to form n-dodecyl groups. The collision ratios of n-dodecane to CH_3, C_2H_5, and 1-C_3H_7 are much higher than those of H, although H attack reactions have higher activity. However, because these three free radicals can be easily generated through the C-C bond cleavage reaction in the process of n-dodecane decomposition, the collision ratio of n-dodecane and

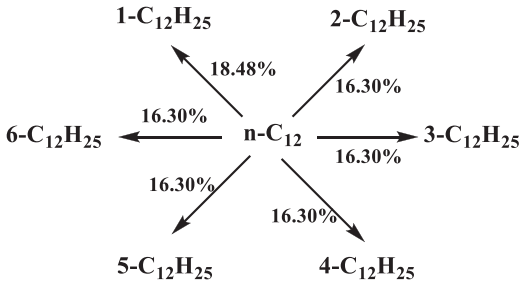

Fig. 16. The flux of n-dodecane initial decomposition pathway at 930 K and 40 atm.

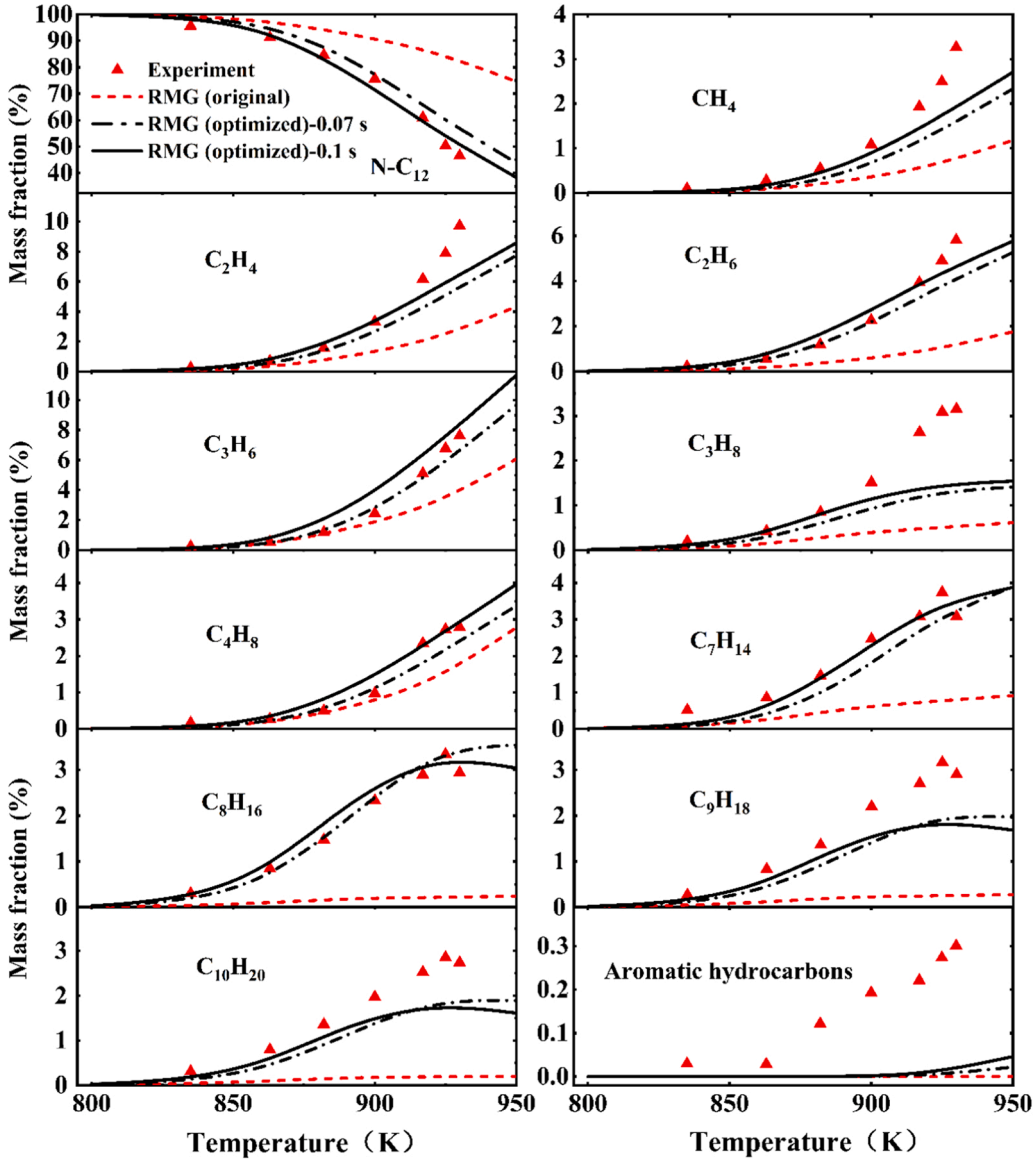

Fig. 15. Comparison of results after mechanism optimization.

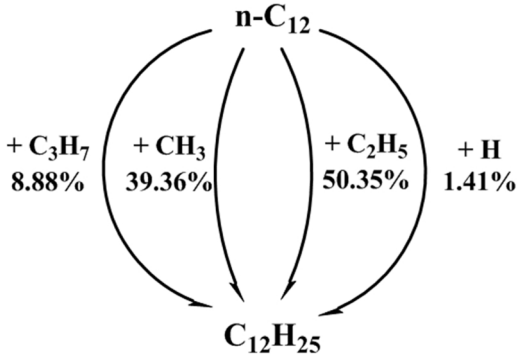

Fig. 17. Participation ratio of each free radical in the initial decomposition of n-dodecane at 930 K and 40 atm.

three carbon-containing free radicals is high.

The pyrolysis conversion of n-dodecane at 930 K and 40 atm has reached 50%, and a large number of gas-liquid cracking products have been produced. The number of n-dodecyl groups produced by the initial decomposition of n-dodecane is large and the reaction path involved is complex. For convenience, taking the n-dodecyl isomer 1-$C_{12}H_{25}$ as an example, the formation of small molecular products will be analyzed in detail in the following section.

5.4. Formation of Small Molecular Products

Fig. 18 shows the reaction pathway flux of 1-$C_{12}H_{25}$ as a demonstration of $C_{12}H_{25}$ decomposition. Only the main cracking pathway is shown in the figure, and the marked ratio number represents the percentage of the reaction rate relative to the total decomposition rate of the substance. Through the path flux analysis, the generation paths and proportions of each product during the decomposition of n-dodecane can be understood more clearly. Many different types of free radicals are generated during the decomposition of 1-n-dodecyl, and these free radicals generate small molecular free radicals and alkenes through further dissociation reactions.

The consumption of 1-n-dodecyl is mainly through H-shift isomerization and β-scissions.

$$1\text{-}C_{12}H_{25} = C_2H_4 + 1\text{-}C_{10}H_{21} \quad \text{(R1)}$$

$$1\text{-}C_{12}H_{25} = 6\text{-}C_{12}H_{25} \quad \text{(R2)}$$

$$1\text{-}C_{12}H_{25} = 5\text{-}C_{12}H_{25} \quad \text{(R3)}$$

Among them, the consumption contributions of R1, R2, and R3 were 36.94%, 42.45%, and 19.65%, respectively. The simulation results are consistent with the calculated results, that is, the activation energy of the H shift is lower than that of the β-scissions [40,41].

1-n-dodecyl undergoes β-scissions to produce ethylene and 1-decyl (1-$C_{10}H_{21}$), and 1-decyl undergoes further isomerization and C-C scission along two reaction paths to generate different alkene 1-C_6H_{12} and 1-C_7H_{14} and free radicals, and then the free radicals can further generate small molecules of ethylene and C_1-C_2 free radicals through dissociation reactions.

1-n-dodecyl produces two n-dodecyl isomers through H-shift isomerization, which can further generate different alkenes and free radicals due to the different positions of the free radicals. Among them, the two decomposition paths of 5-n-dodecyl mainly generate alkenes 1-C_7H_{14} and 1-C_8H_{16}, as well as C_4 and C_5 free radicals, and the two decomposition paths of 6-n-dodecyl mainly generate alkenes 1-C_6H_{12} and 1-C_9H_{18} and C_3 and C_6 free radicals. And then these smaller alkenes and free radicals will be further decomposed to generate small molecules of ethylene, ethane, and other substances.

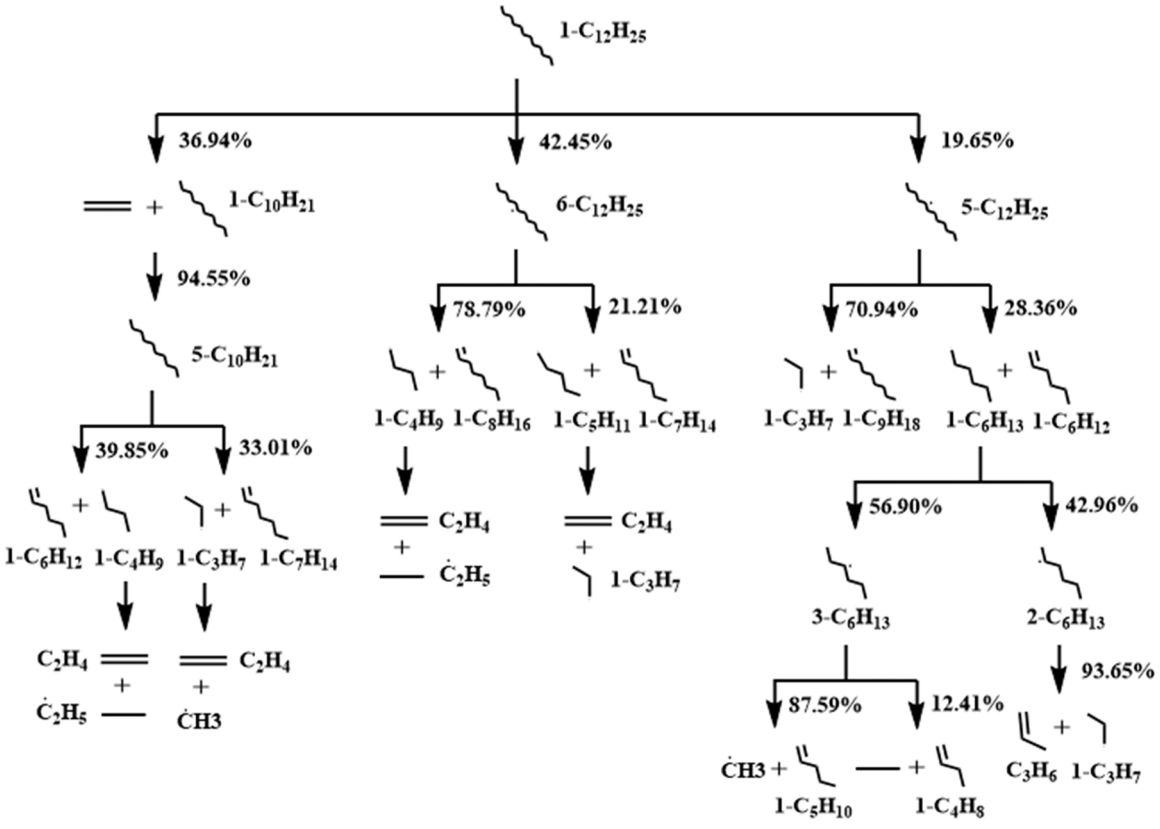

Fig. 18. Reaction pathway flux of 1-$C_{12}H_{25}$ at 930 K and 40 atm.

6. Concluding remarks

In this paper, cracking experiments of n-dodecane at 830–930 K and 40 atm were carried out, and a detailed kinetic model was established with RMG and simulated in CHEMKIN. Contrastively, the LLNL mechanism, JetSurf mechanism and CRECK mechanism were also simulated in CHEMKIN. After the preliminary analysis and comparison of the experiment and simulation, the RMG mechanism was optimized. The preliminary conclusions are as follows:

1) From the experimental and simulation results, when the temperature is higher than 830 K, n-dodecane begins to thermal cracking, and the degree of cracking increases with increasing temperature. When the pyrolysis temperature is below 890 K, the main pyrolysis products are macromolecular olefin. With the increase of pyrolysis temperature, the proportion of small olefin and alkane increased. Under high temperature conditions, the cracking of n-dodecane is more thorough, and the cracking degree reached 53.5% at the pyrolysis temperature of 930 K. The proportion of each gas product to the total gas products is almost constant in the whole temperature range except the lowest temperature 830 K, while the proportion of each liquid product to the total liquid products present the same phenomenon.
2) Compared with the experiment, the simulation results of the four mechanisms widely used for reference have basically the same variation trend of the pyrolysis products, but there are still large disparities. Underestimation of almost products occurs for LLNL mechanism, JetSurf mechanism and RMG mechanism, while overestimation occurs for CRECK mechanism. Moreover, some major products such as C_8H_{16} and C_9H_{18} are absent in CRECK mechanism.
3) The optimized RMG mechanism achieved good agreement with the experimental data. The primary decomposition of n-dodecane is mainly through the H-abstraction reaction with small-molecule free radicals, especially CH_3 and C_2H_5. The H-abstraction reaction results into 6 isomers of n-dodecyl. The consumption of n-dodecyl is mainly through H-shift isomerization and β-scissions, which mainly influence the distributions of pyrolysis products.

By comparing the optimized mechanism simulation results with the experimental data, there are still small differences between the kinetic simulation and the experimental results. Future work will continue to improve the RMG mechanism. Furthermore, it can supplement the mechanism of hydrocarbon fuel pyrolysis under high pressure. In terms of aromatic hydrocarbons, the predictions by all four mechanisms in the paper deviate in order of magnitude with the experimental results, which needs further improvement in the future.

CRediT authorship contribution statement

Zhang Taichang: Conceptualization, Methodology, Formal analysis, Writing – review & editing, Visualization, Supervision, Funding acquisition. **Li Yik:** Resources, Validation, Writing – review & editing. **Zhang Jiahe:** Formal analysis, Investigation, Data curation, Writing – review & editing, Visualization. **Li Yujun:** Software, Investigation, Methodology. **Zhang Dawei:** Resources. **Cui Naifu:** Investigation. **Wu Kun:** Validation, Writing – review & editing. **Fan Xuejun:** Project administration, Funding acquisition.

Declaration of Competing Interest

The authors declare that they have no known competing financial interests or personal relationships that could have appeared to influence the work reported in this paper.

Data Availability

Data will be made available on request.

Acknowledgements

We thank Professor Wang Qingfa of Tianjin University for analyzing the pyrolysis products. This research was supported by the Strategic Leading Science and Technology Special Fund of the Chinese Academy of Sciences (XDA17030100), the Science and Technology Innovation Special Zone Project, and the National Key Project (GJXM92579).

Appendix A. Supporting information

Supplementary data associated with this article can be found in the online version at doi:10.1016/j.jaap.2023.105908.

References

[1] F. Zhong, X. Fan, G. Yu, et al., Thermal cracking and heat sink capacity of aviation kerosene under supercritical conditions, J. Thermophys. Heat. Transf. 25 (3) (2011) 450–456.
[2] X. Fan, G. Yu, J. Li, et al., Combustion and ignition of thermally cracked kerosene in supersonic model combustors, J. Propuls. Power 23 (2) (2007) 317–324.
[3] O. Herbinet, P.-M. Marquaire, F. Battin-Leclerc, et al., Thermal decomposition of n-dodecane: experiments and kinetic modeling, J. Anal. Appl. Pyrolysis 78 (2) (2007) 419–429.
[4] S. Humer, A. Frassoldati, S. Granata, et al., Experimental and kinetic modeling study of combustion of JP-8, its surrogates and reference components in laminar nonpremixed flows, Proc. Combust. Inst. 31 (1) (2007) 393–400.
[5] D. Zhang, L. Hou, J. Liu, et al., Surrogate models of thermally cracked hydrocarbon fuels at typical pyrolysis temperatures, Fuel (2021) 293.
[6] P. Dagaut, On the kinetics of hydrocarbons oxidation from natural gas to kerosene and diesel fuel, Fuel Energy Abstracts 44 (4) (2003) 216.
[7] E. Daniau, M. Bouchez, R. Bounaceur, et al., Contribution to scramjet active cooling analysis using n-dodecane decomposition model, 12th AIAA Int. Space Planes Hypersonic Syst. Technol. (2003), https://doi.org/10.2514/6.2003-6920.
[8] J.Q. Xu, J.J. Guo, A.K. Liu, et al., Construction of autoignition mechanisms for the combustion of RP-3 surrogate fuel and kinetics simulation, Acta Phys. -Chim. Sin. 31 (4) (2015) 643–652.
[9] E.M. Yoon, L. Selvaraj, S. Eser, et al., High-temperature stabilizers for jet fuels and similar hydrocarbon mixtures. 2. kinetic studies, Energy Fuels 10 (3) (1996) 812–815.
[10] E.M. Yoon, L. Selvaraj, C. Song, et al., High-temperature stabilizers for jet fuels and similar hydrocarbon mixtures. 1. comparative studies of hydrogen donors, Energy Fuels 10 (3) (1996) 806–811.
[11] K.D. Dahm, P.S. Virk, R. Bounaceur, et al., Experimental and modelling investigation of the thermal decomposition of n-dodecane, J. Anal. Appl. Pyrolysis 71 (2) (2004) 865–881.
[12] C.K. Westbrook, W.J. Pitz, O. Herbinet, et al., A comprehensive detailed chemical kinetic reaction mechanism for combustion of n-alkane hydrocarbons from n-octane to n-hexadecane, Combust. Flame 156 (1) (2009) 181–199.
[13] S. Banerjee, R. Tangko, D.A. Sheen, et al., An experimental and kinetic modeling study of n-dodecane pyrolysis and oxidation, Combust. Flame 163 (2016) 12–30.
[14] D. Zhang, L. Hou, M. Gao, et al., Experiment and modeling on thermal cracking of n-dodecane at supercritical pressure, Energy Fuels 32 (12) (2018) 12426–12434.
[15] P.X. Jiang, Y.Y. Wang, Y.H. Zhu, Differential global reaction model with variable stoichiometric coefficients for thermal cracking of n-decane at supercritical pressures, Energy Fuels 33 (8) (2019) 7244–7256.
[16] Y.S. Wang, P.X. Jiang, Y.H. Zhu, A novel global reaction modeling approach considering the effects of pressure on pyrolysis of n-decane at supercritical pressures, Fuel 287 (2021), 119416.
[17] L. Zhang, R. Yin, J. Wang, et al., Numerical investigations on the molecular reaction model for thermal cracking of n-decane at supercritical pressures, ACS Omega 7 (26) (2022) 22351–22362.
[18] R. Wang, J. Zhao, Z. Bao, Thermal cracking and coke deposition characteristics of aviation kerosene RP-3 in an S-bend tube, Fuel (2022) 313.
[19] Wang X.Z., Zhang T.C., Lu Y., et al. An Iterative Analysis and Design Method for Study of Coupling Processes of Combustion and Heat Transfer in Actively-Cooled Scramjet Combustor [J]. Journal of Propulsion Technology, 2014.
[20] A. Anderko, 4 Cubic and generalized van der waals equations, in: J.V. Sengers, R. F. Kayser, C.J. Peters, et al. (Eds.), Experimental Thermodynamics, Elsevier, 2000, pp. 75–126.
[21] D.-Y. Peng, D.B. Robinson, A new two-constant equation of state, Ind. Eng. Chem. Fundam. 15 (1) (1976) 59–64.
[22] M.L. Spiegel, S. Liu, J. Schaum's, Outline of Mathematical Handbook of Formulas and Tables, Third ed., McGraw-Hill, 2008.
[23] G. Soave, Equilibrium constants from a modified Redlich-Kwong equation of state, Chem. Eng. Sci. 27 (6) (1972) 1197–1203.
[24] R. Jiang, The high-pressure thermal cracking of endothermic hydrocarbon fuel in microchannel, Dr. Diss. (2012).
[25] C.W. Gao, J.W. Allen, W.H. Green, et al., Reaction mechanism generator: automatic construction of chemical kinetic mechanisms, Comput. Phys. Commun. 203 (2016) 212–225.
[26] R.G. Susnow, A.M. Dean, W.H. Green, et al., Rate-based construction of kinetic models for complex systems, J. Phys. Chem. A 101 (20) (1997) 3731–3740.

[27] S.W. Benson, Methods for the estimation of thermochemical data and rate parameters, Thermochem. Kinet. (1976).
[28] Magoon G., Green W., Oluwole O., et al. Updating Our Understanding of JP-10 Decomposition Chemistry: A Detailed JP-10 Combustion Mechanism Constructed Using RMG, an Automatic Reaction Mechanism Generator [Z]. 46th AIAA/ASME/SAE/ASEE Joint Propulsion Conference & Exhibit. 2010.10.2514/6.2010–6825.
[29] R.J. Kee, F.M. Rupley, J.A. Miller, I.I. CHEMKIN, A fortran chemical kinetics package for the analysis of gas-phase chemical kinetics, Tech. Libr. Process. (1992).
[30] E. Ranzi, A. Frassoldati, S. Granata, et al., Wide-range kinetic modeling study of the pyrolysis, partial oxidation, and combustion of heavy n-alkanes, Ind. Eng. Chem. Res. 44 (14) (2005) 5170–5183.
[31] B. Sirjean, E. Dames, D.A. Sheen, et al., A high-temperature chemical kinetic model of n-alkane oxidation, JetSurF Version 10 (2009).
[32] C.W. Gao, A.G. Vandeputte, N.W. Yee, et al., JP-10 combustion studied with shock tube experiments and modeled with automatic reaction mechanism generation, Combust. Flame 162 (8) (2015) 3115–3129.
[33] A. Stagni, A. Frassoldati, A. Cuoci, et al., Skeletal mechanism reduction through species-targeted sensitivity analysis, Combust. Flame 163 (2016) 382–393.
[34] N. Gascoin, P. Gillard, S. Bernard, et al., Characterisation of coking activity during supercritical hydrocarbon pyrolysis, Fuel Process. Technol. 89 (2008) 1416–1628.
[35] Y. Li, Y. Zhang, R. Zhan, et al., Experimental and kinetic modeling study of ammonia addition on PAH characteristics in premixed n-heptane flames, Fuel Process. Technol. (2021) 214.
[36] L. Cai, H. Pitsch, Mechanism optimization based on reaction rate rules, Combust. Flame 161 (2) (2014) 405–415.
[37] L. Cai, H. Pitsch, S.Y. Mohamed, et al., Optimized reaction mechanism rate rules for ignition of normal alkanes, Combust. Flame 173 (2016) 468–482.
[38] Z. Jia, H. Huang, W. Zhou, et al., Experimental and modeling investigation of n-decane pyrolysis at supercritical pressures, Energy Fuels 28 (9) (2014) 6019–6028.
[39] J. Yu, S. Eser, Thermal decomposition of C10−C14 normal alkanes in near-critical and supercritical regions: product distributions and reaction mechanisms, Ind. Eng. Chem. Res. 36 (3) (1997) 574–584.
[40] D. Healy, N.S. Donato, C.J. Aul, et al., n-Butane: ignition delay measurements at high pressure and detailed chemical kinetic simulations, Combust. Flame 157 (8) (2010) 1526–1539.
[41] D. Healy, N.S. Donato, C.J. Aul, et al., Isobutane ignition delay time measurements at high pressure and detailed chemical kinetic simulations, Combust. Flame 157 (8) (2010) 1540–1551.